MDPI

Joint Trajectory Planning, Time and Power Allocation to Maximize Throughput in UAV Network

Kehao Wang [1,*], **Jiangwei Xu** [1], **Xiaobai Li** [2], **Pei Liu** [1,3], **Hui Cao** [1] and **Kezhong Liu** [4]

1   School of Information Engineering, Wuhan University of Technology, Wuhan 430070, China
2   Air Force Early Warning Academy , Wuhan 430019, China
3   Integrated Computing and Chip Security Sichuan Collaborative Innovation Center, Chengdu University of Information Technology, Chengdu 610059, China
4   School of Navigation, Wuhan University of Technology, Wuhan 430070, China
*   Correspondence: kehao.wang@whut.edu.cn

Abstract: Due to the advantages of strong mobility, flexible deployment, and low cost, unmanned aerial vehicles (UAVs) are widely used in various industries. As a flying relay, UAVs can establish line-of-sight (LOS) links for different scenarios, effectively improving communication quality. In this paper, considering the limited energy budget of UAVs and the existence of multiple jammers, we introduce a simultaneous wireless information and power transfer (SWIPT) technology and study the problems of joint-trajectory planning, time, and power allocation to increase communication performance. Specifically, the network includes multiple UAVs, source nodes (SNs), destination nodes (DNs), and jammers. We assume that the UAVs need to communicate with DNs, the SNs use the SWIPT technology to transmit wireless energy and information to UAVs, and the jammers can interfere with the channel from UAVs to DNs. In this network, our target was to maximize the throughput of DNs by optimizing the UAV's trajectory, time, and power allocation under the constraints of jammers and the actual motion of UAVs (including UAV energy budget, maximum speed, and anti-collision constraints). Since the formulated problem was non-convex and difficult to solve directly, we first decomposed the original problem into three subproblems. We then solved the subproblems by applying a successive convex optimization technology and a slack variables method. Finally, an efficient joint optimization algorithm was proposed to obtain a sub-optimal solution by using a block coordinate descent method. Simulation results indicated that the proposed algorithm has better performance than the four baseline schemes.

Keywords: UAV network; trajectory planning; power allocation; time allocation

1. Introduction

In recent years, due to high mobility, flexible deployment, and low cost, UAVs have been widely used in many scenarios, such as intelligent transportation systems [1–3], disaster relief, military activities, emergency communications, and so on [4–6]. In particular, with the development of 5G technology, non-terrestrial networks have become the next hot spot [7]. For example, [8] studied the extreme performance of a cognitive uplink fixed satellite service and a fixed terrestrial service in the Ka-band 27.5–29.5 GHz frequency range. Ref. [9] studied the physical layer security problem of a satellite network.

Compared with traditional communication methods, most of the wireless communication channels in UAV networks are dominated by line-of-sight (LOS) links [10], which can reduce the obstruction of mountains and buildings so as to obtain better data transmission effects. For example, for natural disasters scenes and ground network communication failures, Ref. [11] used UAVs to provide support for ground base stations and proposed an adaptive UAV deployment scheme to solve the communication network coverage problem. Ref. [12] proposed a task-driven routing strategy for emergency UAVs network to enhance rescue efficiency. Aiming at the post-disaster areas where infrastructure has been destroyed,

Ref. [13] proposed an efficient data transmission scheme based on a particle swarm algorithm to ensure communication quality. Ref. [14] studied a UAV deployment strategy for disaster-affected areas to maximize the number of communication-coverage nodes.

Despite the widespread adoption of UAV-assisted communication technologies, there are still some challenges in UAV networks. First, due to the openness of a UAV network interface and the broadcast nature of electromagnetic waves, a UAV network is susceptible to radio interference. For instance, the existence of malicious jammers could reduce the communication quality between the nodes in a UAV network. Second, the battery capacity of the UAV is limited, which greatly shortens total mission time [15–17].

In view of the problem that a UAV network is susceptible to radio interference, the high mobility of UAVs could be used to improve a system's performance through the reasonable optimization of network resources [18–21]. Whereas, in a UAV network, the resources are limited, coupled with each other, and the established problems are usually non-convex and difficult to solve. Therefore, it is necessary to design a feasible optimization algorithm to obtain a solution to the original problem. Based on this, a successive convex approximation (SCA) [22] can be used as an effective method to solve the original non-convex problem.

To address the problem that the battery capacity of the UAV is limited, traditional energy harvesting mechanisms represented by solar and wind energy have been extensively studied [23,24]. For example, Ref. [23] studied the energy efficiency problem in solar-powered UAV systems by optimizing the speed, acceleration, heading angle, and transmission power of a UAV. Ref. [24] proposed an energy harvesting model based on hybrid solar and wind power for a UAV system and obtained a solution to the signal-to-noise ratio (SNR) outage minimization problem. Unfortunately, due to the limitations of hardware technology, the traditional energy harvesting scheme will significantly increase the take-off weight and lead to the degradation of the system's performance. Based on that, radio frequency (RF)-based SWIPT technology combined with UAV network resource allocation optimization could provide an effective solution [25].

To be specific, SWIPT is a technology that integrates wireless power transfer (WPT) and wireless information transfer (WIT). The power and information could be transferred at the same time, as an RF signal carries both power and information [26]. Typically, time switching (TS) and power splitting (PS) protocols are two common methods to implement SWIPT [27]. The former depends on time-slot allocation, where part of the time slot is used for energy transmission, and the other is used for information transmission and processing. The latter depends on power allocation, where part of the power is used for information transmission and processing, and the other is used for energy harvesting (EH).

1.1. Related Work

For UAV-assisted communication networks, due to the broadcast characteristics of electromagnetic waves, the UAV network is vulnerable to malicious interference. Generally speaking, an attack on the jammers on a UAV communication channel usually focuses on the physical layer and is completed by transmitting high-power interference signals. Therefore, many optimization schemes have been proposed to improve the system's performance.

Based on the high mobility of UAVs, Refs. [28–31] studied the UAV communication system in jamming environments from the perspective of trajectory planning. In [28], the authors studied a dual-UAV communication system with malicious interference and minimized the flight time by optimizing the UAV trajectory with steering angle constraints under the premise of meeting the information transmission requirements. In the scenario with a dynamic jammer, Ref. [29] proposed an offline algorithm based on deep reinforcement learning to optimize the trajectory and minimize the mission completion time. To ensure the reliability of the communication link, Ref. [30] maximized the average SINR by planning a trajectory for UAVs under energy constraints. In [31], the authors studied a UAV communication network with multiple jammers and optimized the UAV's trajectory by using the Dinklebach method and a non-convex optimization method to maximize the energy efficiency of the system.

However, the research on UAV network channel optimization in the above-mentioned interference environment mainly focused on trajectory planning in the space domain. Considering more degrees of freedom for a UAV network, Refs. [32–34] studied the multi-domain optimization problem based on trajectory planning. In [32], the authors mitigated the influence of jammers by jointly optimizing the UAV trajectory and signal transmission power and maximizing the average-secrecy rate of an uplink and a downlink. For the probabilistic LOS channel system, Ref. [33] studied a single UAV-assisted dual-user anti-jamming network and maximized the system throughput by optimizing the UAV's three-dimensional position and the ground nodes' signal transmission power, wherein the UAV provides communication services for two users. In the scenario where jammers have imperfect locations, considering the different requirements for service quality, Ref. [34] maximized the minimum throughput, the average throughput, and the minimum throughput with delay constraints on all nodes by optimizing the UAV trajectory, the task scheduling, and the ground nodes' signal transmission power, based on a successive convex approximation method and a block coordinate descent method. In addition, for the application scenarios of drones in package delivery, Ref. [35] maximized delivery and sensing utility under energy constraints by jointly optimizing the route selection, sensing time, and delivery weight allocation.

Moreover, on account of the fact that an RF signal carries both power and information, many resource allocation schemes were proposed to make the best of finite energy based on RF energy harvesting technology.

Aiming at the vulnerability of the UAV network, some existing works optimized UAV channel quality in terms of security [25,36–38]. In [36], the authors proposed a scheme based on power division and time switching to improve the security rate in a single UAV relay system with eavesdroppers. To analyze the security of the physical layer, Ref. [37] considered three attack scenarios: (1) a free-space optical eavesdropping attack, (2) a radio frequency attack, and (3) both a free-space optical and a radio frequency attack. The authors further studied the effects of SWIPT parameters and power amplifier efficiency on the security of the system. In [25], the authors investigated two cooperative UAV-assisted SWIPT networks. Specifically, they aimed to maximize the average-secrecy rate by jointly optimizing the trajectory and power of the UAVs, as well as the PS ratio. In the scenario where multiple eavesdroppers have imperfect locations, Ref. [38] improved the security of the network by jointly optimizing the UAV's position, noise power, PS, and TS ratios.

In addition, outage probability (OP) describes the probability of link failure and is often used to evaluate the performance of SWIPT communication systems. In [39], the authors obtained the closed-form expressions of outage probability and the bit-error rate in a UAV-relay-assisted decode and forward (DF) network based on TS and PS protocols and analyzed the transmission rate and delay limitation state. Moreover, a fast convergence algorithm based on bandwidth and time allocation was proposed by [40] to optimize the outage probability. In [41], the authors derived closed expressions of OP and throughput over Nakagami-m fading channels in a DF two-way relay system. They also analyzed the effects of the PS factor, threshold, fading severity, and parameters on the network's performance, wherein the two source nodes could communicate with each other with the help of a relay. Also exploiting SWIPT, Ref. [42] proposed a novel UAV-relay-assisted amplifiers and forwards (AF) network and derived connection- and secrecy-outage probabilities based on a PS scheme.

Furthermore, considering the energy-constrained system, some existing works studied the energy efficiency (EE) of networks. In [43], the energy efficiency was maximized by optimizing the UAV position. However, the authors did not use the detailed energy consumption expression of the rotary-wing UAV, but simply adopted the constant power. Ref. [44] investigated a UAV-assisted non-orthogonal multiple access (NOMA) networks, where the Dinkelbach method and successive convex optimization techniques were used to maximize the energy efficiency of the system by designing a UAV's location, beam pattern, power, and time schedule. For a multi-user distributed antenna system, Ref. [45]

maximized the energy efficiency by jointly-optimizing energy allocation and a PS ratio based on the Lagrangian method. Ref. [46] explored SWIPT techniques for device-to-device (D2D) communications based on a nonlinear energy system, optimized power, and the PS ratio maximizing energy efficiency.

Meanwhile, as a promising technology, intelligent reflecting surface (IRS)-aided SWIPT in UAV networks has drawn much attention recently [47,48]. In [47], the authors studied a UAV network supported by IRS and SWIPT and proposed an alternating optimization (AO) algorithm to minimize all users' energy consumption. Moreover, the authors in [48] investigated a UAV network equipped with IRS-aided SWIPT and developed an efficient iterative algorithm based on successive convex approximation, block coordinate descent, and time division multiple access (TDMA) protocols, to maximize the average-transmission rate. Aiming at the security problem in an aerial intelligent reflecting surface (AIRS) network, Ref. [49] proposed an AO algorithm based on the Riemannian manifold optimization method, the SCA technique, and the element-wise BCD method to jointly design the AIRS's deployment and phase shift, so as to maximize the system's secrecy rate.

In addition to the joint UAV trajectory planning and resource allocation optimization methods mentioned above, some existing works proposed new optimization methods to support a UAV communication network [50–52]. For example, considering the trajectory planning problem of multi-UAV assisted networks in a post-disaster scenario, Ref. [50] studied two heuristic algorithms to effectively utilize the UAVs' energy, to improve the communication coverage performance. In the RIS-based UAV-assisted IoT communication scenario, Ref. [51] proposed a multi-UAV path planning/transmission scheduling algorithm based on model predictive control (MPC) to improve system performance and reduce the total energy consumption of UAVs. For the UAV-assisted mobile edge computing (MEC) network communication scenario, Ref. [52] proposed a multi-agent deep reinforcement learning-based UAV trajectory control algorithm to jointly optimize the geographical fairness among all the user equipment, the fairness of every user-equipment load and the users' energy.

1.2. Motivation

In spite of the fact that the related works above have made great progress, there are still several problems needing to be resolved. To be specific, most existing studies did not consider the existence of multiple jammers, even though jammers have a significant impact on the legitimate communication of the system. In addition, most of the existing works considered a single UAV or a single ground node. That is because a multi-UAV system needs to meet a series of requirements, such as an anti-collision constraint and mission planning. These will increase the design difficulty and further increase the complexity of the algorithm. Furthermore, most existing works based on a SWIPT network focused on optimizing power or trajectory instead of multi-domains, including time, power, and trajectory. Most importantly, due to the development of onboard batteries, the flight time of UAVs is limited. The energy constraint problem greatly restricts further applications of UAVs. Therefore, how to improve the communication quality of a UAV network has always been a difficult and hot issue.

Inspired by the discussion above, we study a multi-UAV-assisted multi-user network system. Specifically, where the SN can send information and energy to the power-limited UAV, and the UAV uses the collected energy to communicate with the DN. It should be noted that there are multiple jammers in the network blocking legitimate communication. Different from the existing network, we introduce multiple UAVs based on SWIPT technology and fully consider the existence of jammers and the energy consumption of UAVs. In addition, due to the complexity of the network, solving this joint optimization problem was a considerable challenge. Thus, we introduced multiple slack variables and used the SCA method to make the original problem satisfy the disciplined convex program (DCP) rules so that the reformulated problem could be solved based on the solver CVX.

1.3. Contributions

For the sake of solving the problems given above, a multi-domain optimization algorithm based on the PS protocol that combines trajectory planning, time allocation, and power splitting is proposed by us. We aim to maximize the throughput by considering all constraints. The main contributions of this paper are as follows:

- We investigate a multi-UAV-assisted multi-user relay network in which the SNs use SWIPT technology to transmit wireless energy and information to UAVs. The UAVs use the collected energy to transmit information to the DNs, with the jammers interfering with legitimate channel communications.
- Our goal was to jointly optimize UAV trajectories, time allocation, and power-splitting factors, to mitigate interference and maximize the system throughput. Given that the original problem is non-convex and difficult to solve directly, we decomposed the original problem into three subproblems based on successive convex approximation, block coordinate descent, and a slack variables method presenting an efficient joint optimization algorithm to obtain a suboptimal solution.
- Simulation results indicate that the proposed scheme had better performance than the four benchmark schemes. In addition, we discuss the impact of the number of jammers and energy budgets on system performance and illustrate the effectiveness of joint trajectory planning, time, and power allocation to mitigate interference.

The rest part of the paper is organized as follows. In Section 2, the system model is introduced. In Section 3, we propose a joint optimization algorithm to solve the original problem. In Section 4, we provide simulation results and some necessary discussions. Finally, Section 5 concludes this paper.

2. System Model

Considering a multi-UAV enabled wireless communication network as shown in Figure 1, which includes K_1 quadcopter UAVs, K_2 source nodes (SNs) and destination nodes (DNs), and multiple jammers. Since each pair of ground nodes (SN and DN) is equipped with a fixed UAV to provide communication services for them, then $K_1 = K_2 = K$. In this system, we assume that the UAVs need to communicate with DNs, and the SNs use SWIPT technology to transmit wireless energy and information to UAVs. Specifically, K SNs stored information and energy. First, all SNs simultaneously send information and energy to the UAV relays, and then, the UAV relays use the collected energy to forward the information to the DNs in DF mode. It is assumed that the SNs, the UAVs, and the DNs are each equipped with a single antenna, the jammers are equipped with K antennas, and the jammers' antennas are aimed at the signal transmission direction of the UAVs [53]. Thus, The jammers which are far away from SNs and closer to UAVs interfere with the channel from UAVs to DNs.

In order to describe the model in mathematical terms, we introduce a 3D Cartesian coordinate system. Suppose the locations of SN k and DN k are $\mathbf{w}_{S_k} = (x_{S_k}, y_{S_k}, 0)$ and $\mathbf{w}_{D_k} = (x_{D_k}, y_{D_k}, 0)$ respectively, $k \in \mathcal{K} = \{1, 2, ..., K\}$. The system contains multiple jammers, denoted as $j \in \mathcal{J} = \{1, 2, ..., J\}$, and the location of the j-th jammer is $\mathbf{w}_j = (x_j, y_j, 0)$. At the same time, we discretize the UAVs mission period T into N time slots with equal length δ, i.e., $\delta = \frac{T}{N}$. Therefore, the position of UAV k flying at a height Z in any time slot $n \in \mathcal{N} = \{1, 2, ..., N\}$ is denoted as $\mathbf{q}_k[n] = (x_k[n], y_k[n])$. Moreover, we assume that the maximum flight speed of the UAV k is $V_{\max}$. Thus, we have the following:

$$\|\mathbf{q}_k[n] - \mathbf{q}_k[n-1]\| \leq V_{\max}\delta, \forall k, n = 2, ..., N. \tag{1}$$

which means that the UAV's speed between two adjacent time slots cannot exceed the maximum speed, where $\|\bullet\|$ represents the Euclidean norm. In addition, the distance

between any two UAVs needs to be greater than a minimum safe distance of $D_{\min}$ to avoid collision and ensure safety. Thus,

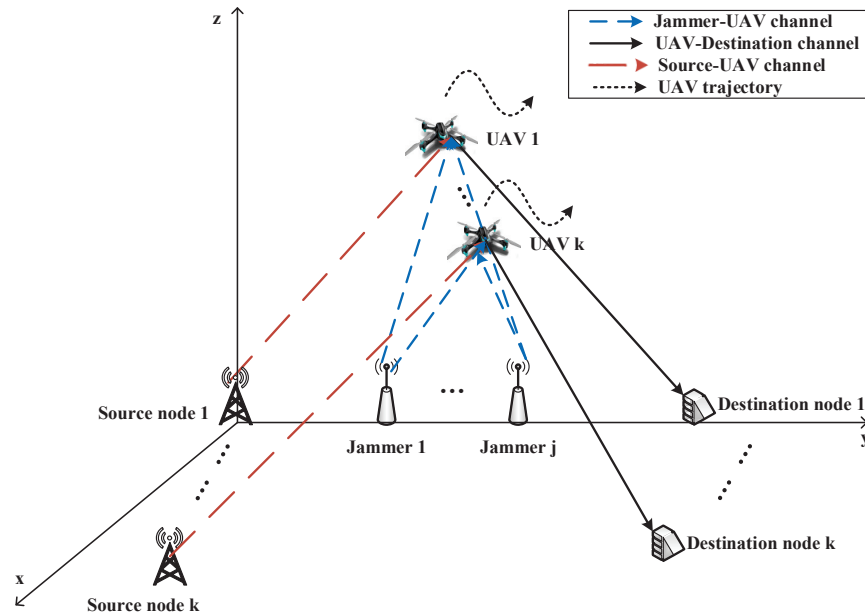$$\|\mathbf{q}_k[n] - \mathbf{q}_l[n]\|^2 \geq D_{\min}^2, \forall k, l, k \neq l. \tag{2}$$

Figure 1. UAV communication network.

Generally speaking, most of the wireless communication channels in UAV networks are dominated by line-of-sight (LOS) links. Thus, following the free-space path loss model, we can get the channel-power gain between SN k and UAV k as follows:

$$h_{S_kU_k}^2 = \beta_{su} \|\mathbf{q}_k[n] - \mathbf{w}_{S_k}\|^{-2} \kappa[n], \forall n. \tag{3}$$

where β_{su} represents SN to UAV channel gain at the reference distance 1 m; $\kappa[n]$ is a small-scale fading with unit mean that is modeled by Rayleigh fading, i.e., $E[|\kappa[n]|^2] = 1$. Similarly, following the free-space path loss model, the channel-power gains from the jammer j to UAV k, and from UAV k to DN k are:

$$h_{jU_k}^2 = \beta_{Ju} \|\mathbf{q}_k[n] - \mathbf{w}_j\|^{-2}, \forall n. \tag{4}$$

$$h_{U_kD_k}^2 = \beta_{ud} \|\mathbf{q}_k[n] - \mathbf{w}_{D_k}\|^{-2}, \forall n. \tag{5}$$

where β_{Ju} and β_{ud} represent jammer j to UAV k and UAV k to DN k channel gain at the reference distance of 1 m, respectively.

2.1. Energy and Information Transmission Model

Inspired by [39], we use the PS protocol to describe the transmission process between the nodes of the network. Specifically, the PS protocol is divided into two steps, as shown in Figure 2, where τ is the time-allocation factor, α is the power-splitting factor, and P_k is the transmit power from SN k to UAV. We first divide each time slot into $\tau\delta$ and $(1-\tau)\delta$. During the first $\tau\delta$ process, the SN sends a signal to the UAV. According to the PS protocol, the $1 - \alpha$ portion of the signal power is used by the UAV to receive and decode a specific signal from the SN, and the remaining portion is used for energy harvesting. Note that the energy collected by UAV from the SN is temporarily stored in the supercapacitor [54]. During the second $(1 - \tau)\delta$ process, the UAV uses the energy collected in the previous stage to transmit the decoded data to the DN. It should be noted that due to the limitation

of energy harvesting efficiency and signal fading, we consider the harvested energy to be only used for signal processing and transmission. The energy consumed by the motor is determined by its own battery capacity, which we will discuss later.
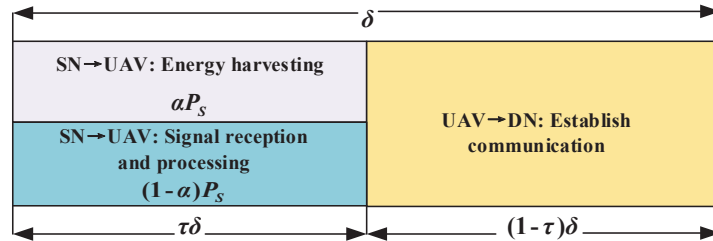

Figure 2. PS protocol.

Based on the above analysis, the UAV-received signal used for information processing during a time slot can be expressed as follows:

$$y_k^{IN} = (1 - \alpha)\sqrt{P_k}h_{S_k U_k}x + n_{su}. \tag{6}$$

where x denotes a signal sent by SN, and n_{su} is additive white Gaussian noise (AWGN) with mean 0 and variance σ_{su}^2, i.e., $n_{su} \sim CN(0, \sigma_{su}^2)$. Therefore, the signal-to-noise ratio (SNR) of the received signal is as follows:

$$SNR_{k_{IN}} = \frac{(1 - \alpha)P_k h_{S_k U_k}^2}{\sigma_{su}^2}. \tag{7}$$

Thus, the achievable rate from SN to UAV is as follows:

$$R_{SU_k} = \tau \log_2\left(1 + SNR_{IN_k}\right), \forall k. \tag{8}$$

It should be noted that in the actual network, the SNR needs to be greater than a threshold γ_{th1}; otherwise, the information transmission will be interrupted. Thus, we have the following:

$$SNR_{IN_k} \geq \gamma_{th1}, \forall k, \forall n. \tag{9}$$

According to the PS protocol, the energy harvesting time during each time slot is $\tau\delta$. Therefore, the energy collected by the UAV in a slot can be expressed as follows:

$$E_k^{EH} = \eta \alpha P_k h_{S_k U_k}^2 \tau \delta. \tag{10}$$

where η is energy collection efficiency. It should be noted that the collected energy cannot exceed the maximum capacity of the supercapacitor. Thus, we have the following:

$$E_k^{EH} \leq E_k^{cap} \tag{11}$$

where E_k^{cap} is the maximum capacity of the supercapacitor. Thus, the UAV's transmission power during the $(1 - \tau)\delta$ can be expressed as follows:

$$P_{U_k} = \frac{E_k^{EH}}{(1 - \tau)\delta} = \frac{\eta \alpha P_k h_{S_k U_k}^2 \tau}{(1 - \tau)}. \tag{12}$$

Due to the existence of the jammers, the received signal-to-interference-plus-noise-ratio (SINR) at the DN needs to be greater than a threshold γ_{th2} to ensure that the signal transmission will not be interrupted. Thus, we have the following:

$$SINR_{D_k} = \frac{P_{U_k}[n]h_{U_k D_k}^2[n]}{\sum_{j=1}^{J} P_j h_{jU_k}^2[n] + \sigma_{ud}^2} \geq \gamma_{th2}, \forall n, \forall k. \tag{13}$$

where σ_{ud}^2 is the noise power, and P_j is the interference power. Thus, the achievable rate from the UAV to the DN is as follows:

$$R_{UD_k} = (1 - \tau)\log_2(1 + SINR_D), \forall k. \tag{14}$$

In addition, the information-causality constraints of the system can be written as

$$\sum_{t=1}^{n} (\tau)\log_2(1 + SNR_{IN_k}) \geq \sum_{t=1}^{n} (1 - \tau)\log_2(1 + SINR_D), n = 1, ..., N, \forall k. \tag{15}$$

2.2. Energy Consumption Model

Compared to energy consumption related to information transmission and signal decoding, UAVs need to consume more energy to maintain level flight. According to existing achievements in [17], the propulsion power of a rotary-wing UAV in 2D horizontal flight could be modeled as

$$P_{uav}(v) = \underbrace{P_B\left(1 + \frac{3v^2}{v_{tip}^2}\right)}_{blade\ profile} + \underbrace{P_I\left(\sqrt{1 + \frac{v^4}{4v_0^4}} - \frac{v^2}{2v_0^4}\right)^{\frac{1}{2}}}_{induced} + \underbrace{\frac{1}{2}d_0\rho s A_0 v^3}_{parasite} \tag{16}$$

where v means the UAV's speed, P_B and P_I are the blade profile and induced powers, respectively, when the UAV is hovering. v_{tip} represents the tip speed of the rotor blade, and v_0 is the mean rotor-induced velocity. In addition, d_0 is the fuselage drag ratio, ρ is the air density, s is rotor solidity, and A_0 is the rotor disc area. Therefore, we can get the sum of the energy consumption of the UAV in a mission period T by

$$E_{UAV}(v) = \int_0^T P_I\left(\sqrt{1 + \frac{v^4}{4v_0^4}} - \frac{v^2}{2v_0^4}\right)^{\frac{1}{2}} dt + \int_0^T P_B\left(1 + \frac{3v^2}{v_{tip}^2}\right) + \frac{1}{2}d_0\rho s A_0 v^3 dt \tag{17}$$

From the definition of time slot δ, we define the UAV's speed as $v = \|\mathbf{q}_k[n] - \mathbf{q}_k[n-1]\|/\delta$. Thus, we can rewrite E_{UAV} as

$$E_{UAV}(\Delta q) = \sum_{n=2}^{N} P_I\left(\sqrt{\delta^4 + \frac{\Delta q^4}{4v_0^4}} - \frac{\Delta q^2}{2v_0^4}\right)^{\frac{1}{2}} + \sum_{n=2}^{N} P_B\left(\delta + \frac{3\Delta q^2}{\delta v_{tip}^2}\right) + \frac{1}{2}d_0\rho s A_0 \frac{\Delta q^3}{\delta^2} \tag{18}$$

where $\Delta q = \|\mathbf{q}_k[n] - \mathbf{q}_k[n-1]\|$. In summary, we get the energy consumption expression of the rotary-wing UAV.

2.3. Problem Formulation

In this paper, our purpose is to maximize the throughput of UAV to the DN by optimizing the trajectory $\mathbf{q}[n]$, time-allocation factor τ, and power-splitting factor α. Thus, the throughput of the DN k over N time slots can be expressed as follows:

$$R_{D_k} = \sum_{n=1}^{N} (1 - \tau)\log_2(1 + SINR_D). \tag{19}$$

Let μ denote the the minimum throughput of DNs, i.e., $\mu = \min_{k \in \mathcal{K}} R_{D_k}$, and define $\mathbf{Q} = \{\mathbf{q}_k[n], \forall k, \forall n\}$, $\boldsymbol{\tau} = \{\tau_k[n], \forall k, \forall n\}$, $\boldsymbol{\alpha} = \{\alpha_k[n], \forall k, \forall n\}$, E_{th} as the UAV's energy budget, and $\mathbf{q}_{start}$ and $\mathbf{q}_{end}$ as the start and endpoints of the UAV. The joint trajectory planning, time, and power allocation optimization problem can be formulated as

$$P1: \max_{\{\mathbf{Q},\boldsymbol{\tau},\boldsymbol{\alpha},\mu\}} \mu \tag{20a}$$

$$s.t. \quad (1), (2), (9), (11), (13), (15) \tag{20b}$$

$$E_{UAV}(\Delta q) \le E_{th}, \forall k \tag{20c}$$

$$\mu \le R_{D_k}, \forall k \tag{20d}$$

$$0 \le \boldsymbol{\tau} \le 1 \tag{20e}$$

$$0 \le \boldsymbol{\alpha} \le 1 \tag{20f}$$

$$\mathbf{q}_k[1] = \mathbf{q}_{start} \tag{20g}$$

$$\mathbf{q}_k[N] = \mathbf{q}_{end} \tag{20h}$$

Note that problem P1 is difficult to solve directly since (2), (11), (13), (15), (20c), and (20d) are non-convex. In the next section, we propose an efficient iterative algorithm to obtain a feasible solution to original problem.

3. Joint Optimization

Since P1 is a non-convex problem, it is difficult to solve directly. In this section, we divide P1 into three subproblems and obtain suboptimal solutions by applying a successive convex approximation and a slack variables method. Then, we develop an overall iterative algorithm based on the block coordinate descent technique to get a locally optimal solution. The specific flow chart is shown in Figure 3.
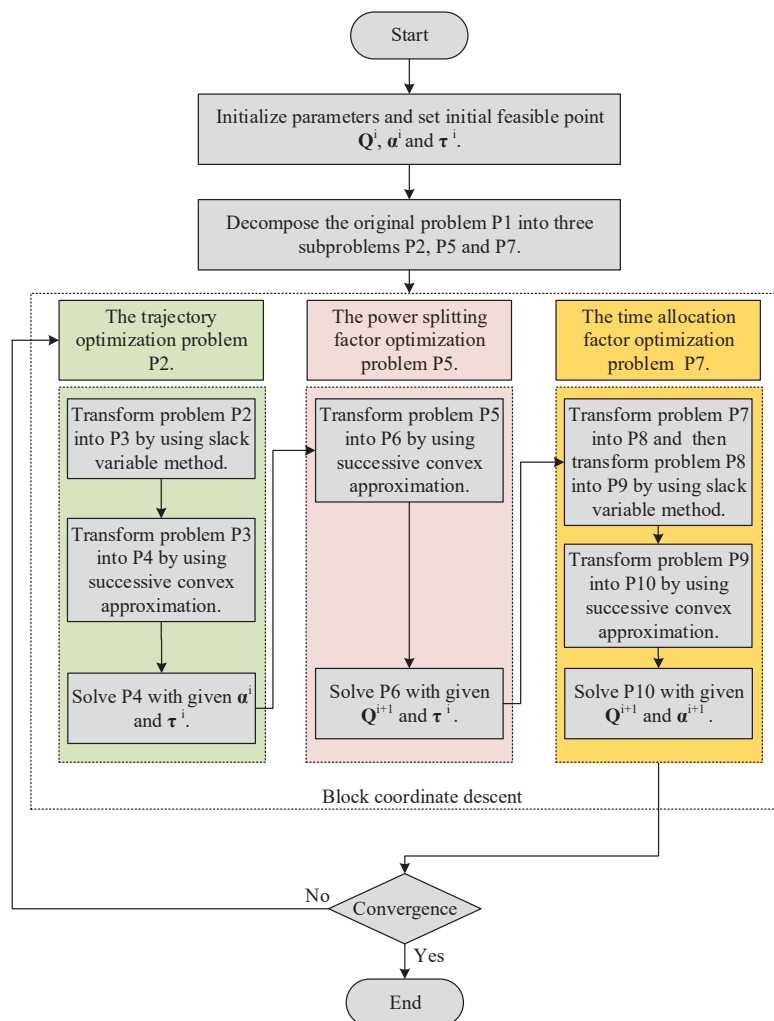

Figure 3. The flow chart of solution to problem P1.

3.1. Optimization of Trajectory

For any fixed power-splitting and time-allocation factors $\{\alpha, \tau\}$, the trajectory optimization problem can be expressed as follows:

$$P2 : \max_{\{\mathbf{Q}, \mu\}} \mu \tag{21a}$$

$$s.t. \quad (1), (2), (9), (11), (13), (15), (20c), (20d), (20g), (20h) \tag{21b}$$

Note that the problem P2 is intractable due to the non-convexity of (2), (11), (13), (15), (20c), and (20d). To tackle this issue, we first introduce slack variables $\{\mathbf{A}[n], \mathbf{B}[n], \mathbf{C}[n]\}$.

Theorem 1. *By introducing slack variables, problem P3 could be equivalently written as*

$$P3 : \max_{\{\mathbf{q}[n], \mu, \mathbf{A}[n], \cdots, \mathbf{D}[n]\}} \mu \tag{22a}$$

$$s.t. \quad (1), (2), (9), (11), (15), (20c), (20g), (20h) \tag{22b}$$

$$\mu \leq \sum_{n=2}^{N} (1 - \tau_k[n]) \log_2 \left(1 + \frac{1}{A_k[n] B_k[n] C_k[n]} \right) \tag{22c}$$

$$A_k[n] \geq \left(\frac{\eta \alpha P_k \beta_{su} \tau_k[n]}{1 - \tau_k[n]} \right)^{-1} \left\| \mathbf{q}_k[n] - \mathbf{w}_{S_k} \right\|^2, \forall k, \forall n \tag{22d}$$

$$B_k[n] \geq \beta_{ud}^{-1} \left\| \mathbf{q}_k[n] - \mathbf{w}_{D_k} \right\|^2, \forall k, \forall n \tag{22e}$$

$$C_k[n] \geq \sum_{j=1}^{J} P_j \beta_{Ju} \left\| \mathbf{q}_k[n] - \mathbf{w}_j \right\|^{-2} + \sigma_{ud}^2, \forall k, \forall n \tag{22f}$$

$$\frac{1}{A_k[n] B_k[n] C_k[n]} \geq \gamma_{th2}, \forall k, \forall n \tag{22g}$$

Proof. The theorem can be proved by the method of contradiction. Specifically, if (22d)–(22f) are strict equality constraints, problem P3 is equal to P2. Otherwise, by adjusting the slack variables, the value of the objective can always be further optimized. □

However, P3 is still difficult to solve because (15), (20c), and (22f) are non-convex constraints, and the left-hand-side (LHS) of (2) and (22g), the right-hand-side (RHS) of (22c) is convex. Consider that any convex function is globally lower-bounded by its first-order Taylor expansion at any point [55]. Therefore, taking Taylor expansion approximately as lower bound, we can obtain the following:

$$\log_2 \left(1 + \frac{1}{\mathbf{A}[n] \mathbf{B}[n] \mathbf{C}[n]} \right) \geq \log_2 \left(1 + \frac{1}{\mathbf{A}^i \mathbf{B}^i \mathbf{C}^i} \right) - \frac{\mathbf{A}[n] - \mathbf{A}^i}{\mathbf{A}^i (1 + \mathbf{A}^i \mathbf{B}^i \mathbf{C}^i) \ln 2}$$
$$- \frac{\mathbf{B}[n] - \mathbf{B}^i}{\mathbf{B}^i (1 + \mathbf{A}^i \mathbf{B}^i \mathbf{C}^i) \ln 2} - \frac{\mathbf{C}[n] - \mathbf{C}^i}{\mathbf{C}^i (1 + \mathbf{A}^i \mathbf{B}^i \mathbf{C}^i) \ln 2} \tag{23}$$

where $(\mathbf{A}^i, \mathbf{B}^i, \mathbf{C}^i)$ is a given local point in the i-th iteration.

Ignoring the terms that are independent of the slack variables $(\mathbf{A}[n], \mathbf{B}[n], \mathbf{C}[n])$, we replace the RHS of (22c) with $\mathbf{S}[n]$:

$$\mathbf{S}[n] = -\frac{\mathbf{A}[n] / \mathbf{A}^i + \mathbf{B}[n] / \mathbf{B}^i + \mathbf{C}[n] / \mathbf{C}^i}{(1 + \mathbf{A}^i \mathbf{B}^i \mathbf{C}^i) \ln 2} \tag{24}$$

$$\mu \leq \sum_{n=2}^{N} (1 - \tau_k[n]) \mathbf{S}[n] \tag{25}$$

Similar to Theorem 1, by introducing slack variables $\mathbf{D}[n]$, (22f) could be equivalently written as follows:

$$C_k[n] \geq \sum_{j=1}^{J} P_j \beta_{Ju} D_{k,j}(n)^{-1} + \sigma_{ud}^2, \forall k, \forall n \tag{26a}$$

$$0 \leq D_{k,j}(n) \leq \left\| \mathbf{q}_k[n] - \mathbf{w}_j \right\|^2, \forall k, \forall n, \forall j \tag{26b}$$

However, we notice that the RHS of (26b) is convex with respect to trajectory $\mathbf{Q}$, thus, (26b) is still a non-convex constraint. Relying on the first-order Taylor expansion, we have the lower bound as

$$\left\| \mathbf{q}_k[n] - \mathbf{w}_j \right\|^2 \geq \left\| \mathbf{q}_k^i[n] - \mathbf{w}_j \right\|^2 + 2(\mathbf{q}_k^i[n] - \mathbf{w}_j)^T \times (\mathbf{q}_k[n] - \mathbf{q}_k^i[n]) = E_{k,j}[n], \forall k, \forall n, \forall j \tag{27}$$

Thus, we reformulate (26b) as

$$0 \leq D_{k,j}(n) \leq E_{k,j}(n), \forall k, \forall n, \forall j \tag{28}$$

For the non-convex constraint (22g). Since the LHS of (22g) is convex, we apply the first-order Taylor expansion to get the lower bound at the i-th iteration point

$$\frac{1}{\mathbf{A}[n]\mathbf{B}[n]\mathbf{C}[n]} \geq \frac{1}{\mathbf{A}^i \mathbf{B}^i \mathbf{C}^i} - \frac{(\mathbf{A}[n] - \mathbf{A}^i)}{(\mathbf{A}^i)^2 \mathbf{B}^i \mathbf{C}^i} - \frac{(\mathbf{B}[n] - \mathbf{B}^i)}{\mathbf{A}^i (\mathbf{B}^i)^2 \mathbf{C}^i} - \frac{(\mathbf{C}[n] - \mathbf{C}^i)}{\mathbf{A}^i \mathbf{B}^i (\mathbf{C}^i)^2} \geq \gamma_{th2} \tag{29}$$

For the LHS of (2), we can obtain the lower bound according to the first-order Taylor expansion as

$$\left\| \mathbf{q}_k[n] - \mathbf{q}_l[n] \right\|^2 \geq - \left\| \mathbf{q}_k^i[n] - \mathbf{q}_l^i[n] \right\|^2 + 2(\mathbf{q}_k^i[n] - \mathbf{q}_l^i[n])^T \times (\mathbf{q}_k[n] - \mathbf{q}_l[n]) \tag{30}$$

Therefore, the non-convex constraint (2) can be rewritten as a convex constraint:

$$\left\| \mathbf{q}_k^i[n] - \mathbf{q}_l^i[n] \right\|^2 + 2(\mathbf{q}_k^i[n] - \mathbf{q}_l^i[n])^T \times (\mathbf{q}_k[n] - \mathbf{q}_l[n]) \geq D_{\min}^2, \forall k, l, k \neq l. \tag{31}$$

For the information-causality constraint (15), by introducing slack variables $\{\mathbf{F}, \mathbf{G}, \mathbf{H}, \mathbf{I}\}$, we have the following:

$$\sum_{t=1}^{n} (\tau) \log_2 \left(1 + \frac{\eta \alpha P_k \tau}{(1-\tau) F_k[t] G_k[t] H_k[t]} \right)$$
$$\leq \sum_{t=1}^{n} (1-\tau) \log_2 \left(1 + \frac{(1-\alpha) P_k}{\sigma^2 I_k[t]} \right), n = 1, ..., N, \forall k. \tag{32a}$$

$$F_k[n] \leq \sum_{j=1}^{J} P_j h_{jU_k}^2[n] + \sigma_{ud}^2, n = 1, ..., N. \tag{32b}$$

$$G_k[n] \leq \beta_{su}^{-1} \left\| \mathbf{q}_k[n] - \mathbf{w}_{S_k} \right\|^2, n = 1, ..., N. \tag{32c}$$

$$H_k[n] \leq \beta_{ud}^{-1} \left\| \mathbf{q}_k[n] - \mathbf{w}_{D_k} \right\|^2, n = 1, ..., N. \tag{32d}$$

$$I_k[n] \geq \beta_{su}^{-1} \left\| \mathbf{q}_k[n] - \mathbf{w}_{S_k} \right\|^2, n = 1, ..., N. \tag{32e}$$

Since the RHS of (32a) is convex with respect to $\mathbf{I}$, relying on the first-order Taylor expansion, we have the following:

$$\log_2 \left(1 + \frac{(1-\alpha) P_k}{\sigma^2 I_k} \right) \geq \log_2 \left(1 + \frac{(1-\alpha) P_k}{\sigma^2 I_k^i} \right) - \frac{(1-\alpha) P_k (I_k - I_k^i)}{\left(\sigma^2 (I_k^i)^2 + (1-\alpha) P_k I_k^i \right) \ln 2} = L \tag{33}$$

Thus, (32a) can be written as

$$\sum_{t=1}^{n} (\tau)\log_2\left(1 + \frac{\eta\alpha P_k\tau}{(1-\tau)F_k[t]G_k[t]H_k[t]}\right) \leq \sum_{t=1}^{n}(1-\tau)L_k[t], n = 1, ..., N, \forall k. \quad (34)$$

For the non-convex constraint (32b), by introducing slack variables **M**, we have:

$$F_k[n] \leq \sum_{j=1}^{J} P_j M_{k,j}[n] + \sigma_{ud}^2, \forall k, \forall n. \quad (35a)$$

$$\frac{1}{M_{k,j}[n]} \geq \beta_{Ju}^{-1}\|\mathbf{q}_k[n] - \mathbf{w}_j\|^2, \forall k, \forall n, \forall j. \quad (35b)$$

Since the LHS of (35b) is convex, we have the following:

$$\frac{1}{M_{k,j}[n]} \geq \frac{1}{M_{k,j}^i[n]} - \frac{M_{k,j}[n] - M_{k,j}[n]}{M_{k,j}^i[n]^2} \geq \beta_{Ju}^{-1}\|\mathbf{q}_k[n] - \mathbf{w}_j\|^2 \quad (36)$$

Similar to (27), for the non-convex constraints (32c) and (32d), we have:

$$\beta_{su}^{-1}\left\|\mathbf{q}_k^i[n] - \mathbf{w}_{S_k}\right\|^2 + 2\beta_{su}^{-1}(\mathbf{q}_k^i[n] - \mathbf{w}_{S_k})^T \times (\mathbf{q}_k[n] - \mathbf{q}_k^i[n]) \geq G_k[n], \forall k, \forall n. \quad (37a)$$

$$\beta_{ud}^{-1}\left\|\mathbf{q}_k^i[n] - \mathbf{w}_{D_k}\right\|^2 + 2\beta_{ud}^{-1}(\mathbf{q}_k^i[n] - \mathbf{w}_{D_k})^T \times (\mathbf{q}_k[n] - \mathbf{q}_k^i[n]) \geq H_k[n], \forall k, \forall n. \quad (37b)$$

Similarly, for the non-convex constraint (11), we have the following:

$$\frac{\eta\alpha P_k\beta_{su}\tau\delta}{E_k^{cap}} \leq \left\|\mathbf{q}_k^i[n] - \mathbf{w}_{S_k}\right\|^2 + 2(\mathbf{q}_k^i[n] - \mathbf{w}_{S_k})^T \times (\mathbf{q}_k[n] - \mathbf{q}_k^i[n]), \forall k, \forall n. \quad (38)$$

Since the energy constraint expression (20c) is very complex and difficult to solve directly, in order to facilitate the analysis, we introduce a slack variable **O** as follows:

$$O_k[n] \geq \left(\sqrt{\delta^4 + \frac{\Delta q_k^4}{4v_0^4}} - \frac{\Delta q_k^2}{2v_0^4}\right)^{\frac{1}{2}} \quad (39)$$

We can further obtain:

$$O_k^2[n] + \frac{\Delta q_k^2}{v_0^2} \geq \frac{\delta^4}{O_k^2[n]}, n = 2, ..., N, \forall k. \quad (40)$$

Therefore, the energy consumption of the UAV k can be equivalently expressed as follows:

$$E_{th} \geq E_k(\Delta q_k, O_k[n]) = \sum_{n=2}^{N} P_B(\delta + \frac{3\Delta q^2}{\delta v_{tip}^2}) + \frac{1}{2}d_0\rho s A_0\frac{\Delta q^3}{\delta^2} + \sum_{n=2}^{N} P_I O_k[n] \geq E_{UAV}(\Delta q_k), \forall k \quad (41)$$

Finally, for non-convex constraint (40), we have the following:

$$O_k^2[n] + \frac{\Delta q_k^2}{v_0^2} \geq O_k^i[n]^2 + \frac{\Delta q_k^i}{v_0^2}^2 + 2O_k^i[n](O_k[n] - O_k^i[n]) + \frac{2\Delta q_k^i}{v_0^2}(\Delta q_k - \Delta q_k^i) \geq \frac{\delta^4}{O_k^2[n]}, \forall k. \quad (42)$$

As a result, the lower bound problem of P3 can be approximated as

$$P4 : \max_{\{\mathbf{Q},\mathbf{A},...,\mathbf{O},\mu\}} \mu \tag{43a}$$

$$s.t. \quad (1),(9),(20g),(20h),(22d),(22e),(25),(26a),(28),(29),$$
$$(31),(32e),(34),(35a),(36),(37a),(37b),(38),(41),(42) \tag{43b}$$

Obviously, P4 is a convex optimization problem that could be solved efficiently by some classical optimization techniques, such as the interior point method. In addition, it is worth noting that the optimal objective value obtained from P4 usually serves as a lower bound of P3.

3.2. Optimization of Power Splitting Factor

For any fixed UAV trajectory and time-allocation factor $\{\mathbf{Q}, \boldsymbol{\tau}\}$, the power-splitting factor optimization problem can be expressed as follows:

$$P5 : \max_{\{\boldsymbol{\alpha},\mu\}} \mu \tag{44a}$$

$$s.t. \quad (9),(11),(13),(15),(20d),(20f) \tag{44b}$$

It should be noted that problem P5 is not a standard convex optimization problem because the LHS and the RHS of (15) are concave. Thus, consider that any concave function is globally upper-bounded by its first-order Taylor expansion. Therefore, we can obtain the following:

$$\log_2(1 + \alpha P) \leq \log_2\left(1 + \alpha^i P\right) + \frac{(\alpha - \alpha^i)P}{(1 + \alpha^i P)\ln 2} \tag{45}$$

where

$$P = \frac{\eta P_k h_{S_k U_k}^2 \tau h_{U_k D_k}^2}{(1 - \tau)\left(\sum\limits_{j=1}^{J} P_j h_{jU_k}^2 + \sigma_{ud}^2\right)} \tag{46}$$

Thus, the lower bound problem of P5 can be approximated as

$$P6 : \max_{\{\boldsymbol{\alpha},\mu\}} \mu \tag{47a}$$

$$s.t. \quad (9),(11),(13),(20d),(20f) \tag{47b}$$

$$\sum_{t=1}^{n} (1 - \tau)\left(\log_2\left(1 + \alpha_k^i[t]P[t]\right) + \frac{(\alpha_k[t] - \alpha_k^i[t])P[t]}{(1 + \alpha_k^i[t]P[t])\ln 2}\right)$$
$$\leq \sum_{t=1}^{n} (\tau)\log_2(1 + SNR_{IN_k}), n = 1,...,N, \forall k. \tag{47c}$$

P6 is also a convex optimization problem that can be solved like P4. Additionally, the optimal objective value obtained from P6 usually serves as a lower bound of P5.

3.3. Optimization of Time-Allocation Factor

For any given power-splitting factor and trajectory $\{\boldsymbol{\alpha}, \mathbf{Q}\}$, we consider the subproblem of optimizing the time-allocation factor as follows:

$$P7 : \max_{\{\boldsymbol{\tau},\mu\}} \mu \tag{48a}$$

$$s.t. \quad (11),(13),(15),(20d),(20e) \tag{48b}$$

Further, we can transform the problem P7 into P8:

$$P8 : \max_{\{\tau,\mu\}} \mu \tag{49a}$$

$$s.t. \ (11),(13),(15),(20e) \tag{49b}$$

$$\mu \leq \sum_{n=1}^{N} (1-\tau_k[n])\log_2\left(1+\frac{\tau_k[n]}{1-\tau_k[n]}R_k[n]\right), \forall k \tag{49c}$$

where

$$R_k[n] = \frac{\alpha_k[n]\eta P_k h_{S_k U_k}^2[n]h_{U_k D_k}^2[n]}{\sum\limits_{J=1}^{J} P_j h_{jU_k}^2[n] + \sigma_{ud}^2} \tag{50}$$

Since (15) and (49c) are non-convex, P8 is difficult to solve directly. To this end, we introduce slack variables to solve this problem.

Theorem 2. *By introducing slack variables* $\{\mathbf{U},\mathbf{V},\mathbf{W},\mathbf{X}\}$*, problem P8 could be equivalently written as follows:*

$$P9 : \max_{\{\tau,\mu,\mathbf{U},...,\mathbf{X}\}} \mu \tag{51a}$$

$$s.t. \ (11),(13),(20e) \tag{51b}$$

$$\mu \leq \sum_{n=1}^{N} U_k[n]V_k[n], \forall k \tag{51c}$$

$$0 \leq U_k[n] \leq 1 - \tau_k[n], \forall k, \forall n \tag{51d}$$

$$0 \leq V_k[n] \leq \log_2\left(1+\frac{\tau_k[n]}{1-\tau_k[n]}R_k[n]\right), \forall k, \forall n \tag{51e}$$

$$W_k[n] \geq 1 - \tau_k[n], \forall k, \forall n \tag{51f}$$

$$X_k[n] \geq \log_2\left(1+\frac{\tau_k[n]}{1-\tau_k[n]}R_k[n]\right), \forall k, \forall n \tag{51g}$$

$$\sum_{t=1}^{n} W_k[t]X_k[t] \leq \sum_{t=1}^{n} (\tau)\log_2(1+SNR_{IN_k}), n = 1,...,N, \forall k. \tag{51h}$$

Proof. According to (51d) and (51e), we have the following:

$$\sum_{n=1}^{N} U_k[n]V_k[n] \leq \sum_{n=1}^{N} (1-\tau_k[n])\log_2\left(1+\frac{\tau_k[n]}{1-\tau_k[n]}R_k[n]\right) \tag{52}$$

According to (51f) and (51g), we have the following:

$$\sum_{t=1}^{n} (1-\tau_k[t])\log_2\left(1+\frac{\tau_k[t]}{1-\tau_k[t]}R_k[t]\right) \leq \sum_{t=1}^{n} W_k[t]X_k[t] \tag{53}$$

Therefore, we prove the theorem by the method of contradiction. Specifically, if (52) and (53) are strict equality constraints, combined with (51c) and (51h), we can know that P9 is equal to P8. Otherwise, by adjusting the slack variables, the value of the objective function can always be further optimized. $\square$

However, P9 is still a non-convex optimization problem that is difficult to solve directly. Considering that (51c) has a product of functions (PF) structure, we can rewrite (51c) as a function with the difference of convex (DC) structure, that is,

$$\mathbf{UV} = \frac{1}{2}(\mathbf{U}+\mathbf{V})^2 - \frac{1}{2}(\mathbf{U}^2+\mathbf{V}^2) \tag{54}$$

Since the first term in the RHS of (54) is convex, we can obtain a lower bound for (54) by using first-order Taylor expansion, that is

$$\frac{1}{2}(\mathbf{U}+\mathbf{V})^2 - \frac{1}{2}(\mathbf{U}^2+\mathbf{V}^2) \geq (\mathbf{U}^i+\mathbf{V}^i)(\mathbf{U}+\mathbf{V}) - \frac{1}{2}(\mathbf{U}^i+\mathbf{V}^i)^2 - \frac{1}{2}(\mathbf{U}^2+\mathbf{V}^2) = \mathbf{Y} \quad (55)$$

Thus, (51c) can be rewritten as

$$\mu \leq \sum_{n=2}^{N} \mathbf{Y} \quad (56)$$

For the non-convex constraint (51e), by introducing slack variables $\mathbf{Z}$, we have:

$$0 \leq V_k[n] \leq \log_2(1 + Z_k[n]R_k[n]) \quad (57\text{a})$$

$$0 \leq Z_k[n] \leq \frac{\tau_k[n]}{1 - \tau_k[n]} \quad (57\text{b})$$

Furthermore, the RHS of the (57b) is convex on the domain ($\tau \in [0,1]$). Thus, we have the following:

$$\frac{\tau_k[n]}{1 - \tau_k[n]} \geq \left(\frac{1}{1 - \tau_k^i[n]} - 1\right) + \frac{\tau_k[n] - \tau_k^i[n]}{\left(1 - \tau_k^i[n]\right)^2} = \mathbf{\Gamma} \quad (58)$$

Thus, (57b) can be rewritten as

$$0 \leq \mathbf{Z} \leq \mathbf{\Gamma} \quad (59)$$

Similar to the procedure of handling (51e), for the non-convex constraint (51g), by introducing the slack variable $\mathbf{\Lambda}$, we have

$$X_k[n] \geq \log_2\left(1 + \frac{R_k[n]}{\mathbf{\Lambda}_k[n]}\right) \quad (60\text{a})$$

$$0 \leq \mathbf{\Lambda}_k[n] \leq \frac{1 - \tau_k[n]}{\tau_k[n]} \quad (60\text{b})$$

For the (60b), we have

$$\frac{1 - \tau_k[n]}{\tau_k[n]} \geq \frac{1}{\tau_k^i[n]} - \frac{\left(\tau_k[n] - \tau_k^i[n]\right)}{\left(\tau_k^i[n]\right)^2} - 1 \geq \mathbf{\Lambda}_k[n] \geq 0 \quad (61)$$

According to (55), for the (51h), we have

$$\sum_{t=1}^{n} \mathbf{W}\mathbf{X} \leq \sum_{t=1}^{n} \frac{1}{2}(\mathbf{W}+\mathbf{X})^2 \leq \sum_{t=1}^{n} (\tau)\log_2(1 + SNR_{IN_k}), n = 1, ..., N, \forall k. \quad (62)$$

As a result, the lower bound problem of P9 can be rewritten as

$$P10: \max_{\{\boldsymbol{\tau}, \mu, \mathbf{U}, ..., \mathbf{\Lambda}\}} \mu \quad (63\text{a})$$

$$s.t. \ (11), (13), (20\text{e}), (51\text{d}), (51\text{f}), (56), (57\text{a}), (59), (60\text{a}), (61), (62) \quad (63\text{b})$$

P10 is also a convex optimization problem that can be solved like P6. In addition, the optimal objective value obtained from P10 usually serves as a lower bound of P9.

3.4. Algorithmic Architecture

According to the above analysis, we obtain the suboptimal solution of the original problem P1 based on the block coordinate descent (BCD) method. As shown in Algorithm 1, the algorithm alternately optimizes $\mathbf{Q}$, $\boldsymbol{\alpha}$, and $\boldsymbol{\tau}$ until convergence. Note that the initial

point is the Taylor expansion point within the feasible region. Then, the convergence is proved as follows:

Algorithm 1 Overall algorithm

1: **Initialize** $i = 1$. Set initial feasible point $\{\mathbf{Q}^i, \boldsymbol{\alpha}^i, \boldsymbol{\tau}^i\}$ and other slack variables.
2: **Do**
3:     Solve problem P4 with given $\{\mathbf{Q}^i, \boldsymbol{\alpha}^i, \mathbf{A}^i, ..., \mathbf{O}^i\}$ to obtain the optimal solution $\{\mathbf{Q}^{i+1}, \mathbf{A}^{i+1}, ..., \mathbf{O}^{i+1}\}$,
4:     Solve problem P6 with given $\{\boldsymbol{\alpha}^i, \mathbf{Q}^{i+1}, \boldsymbol{\tau}^i\}$ to obtain the optimal solution $\{\boldsymbol{\alpha}^{i+1}\}$,
5:     Solve problem P10 with given $\{\boldsymbol{\alpha}^{i+1}, \mathbf{Q}^{i+1}, ..., \boldsymbol{\Lambda}^i\}$ to obtain the optimal solution $\{\boldsymbol{\tau}^{i+1}, ..., \boldsymbol{\Lambda}^{i+1}\}$.
6:     **Update** $i = i + 1$.
7: **Until** the objective value converges.
8: **Output** $\boldsymbol{\alpha}^* \leftarrow \boldsymbol{\alpha}^i, \mathbf{Q}^* \leftarrow \mathbf{Q}^i, \boldsymbol{\tau}^* \leftarrow \boldsymbol{\tau}^i$.

We define $\mu(\mathbf{Q}^i, \boldsymbol{\alpha}^i, \boldsymbol{\tau}^i)$, $\mu_1(\mathbf{Q}^i, \boldsymbol{\alpha}^i, \boldsymbol{\tau}^i)$, $\mu_2(\mathbf{Q}^i, \boldsymbol{\alpha}^i, \boldsymbol{\tau}^i)$, and $\mu_3(\mathbf{Q}^i, \boldsymbol{\alpha}^i, \boldsymbol{\tau}^i)$ as the objective values of problem P1, P4, P6 and P10 based on $\mathbf{Q}^i$, $\boldsymbol{\alpha}^i$, and $\boldsymbol{\tau}^i$ over i-th iteration. Thus, we have

$$\mu(\mathbf{Q}^i, \boldsymbol{\alpha}^i, \boldsymbol{\tau}^i) \overset{(a)}{\leq} \mu_1(\mathbf{Q}^{i+1}, \boldsymbol{\alpha}^i, \boldsymbol{\tau}^i) \overset{(b)}{\leq} \mu_2(\mathbf{Q}^{i+1}, \boldsymbol{\alpha}^{i+1}, \boldsymbol{\tau}^i)$$
$$\overset{(c)}{\leq} \mu_3(\mathbf{Q}^{i+1}, \boldsymbol{\alpha}^{i+1}, \boldsymbol{\tau}^{i+1}) \overset{(d)}{\leq} \mu(\mathbf{Q}^{i+1}, \boldsymbol{\alpha}^{i+1}, \boldsymbol{\tau}^{i+1}) \tag{64}$$

where (a) holds because in Algorithm 1, problem P4 is solved to obtain the optimal solution $\mathbf{Q}^{i+1}$ with given $\boldsymbol{\alpha}^i$ and $\boldsymbol{\tau}^i$ at step 3; (b) holds because problem P6 is solved to obtain the optimal solution $\boldsymbol{\alpha}^{i+1}$ with given $\mathbf{Q}^{i+1}$ and $\boldsymbol{\tau}^i$ at step 4; (c) holds because problem P10 is solved to obtain the optimal solution $\boldsymbol{\tau}^{i+1}$ with given $\mathbf{Q}^{i+1}$ and $\boldsymbol{\alpha}^{i+1}$ at step 5; (d) holds because the optimal objective values of P4, P6 and P10 are upper bounded by original problem P1, then the convergence can be guaranteed.

Finally, we briefly analyze the overall complexity of the algorithm. According to Algorithm 1, the complexity of the algorithm is mainly dominated by steps 3, 4, and 5, and the number of optimization variables increases with the multiples of K, J, and N. Hence, the total computational complexity is $O((KJN)^{3.5} \log \frac{1}{\varepsilon})$, where K is the number of UAVs, J is the number of jammers, N is the number of time slots, and ε is the convergence accuracy. In addition, it should be noted that the proposed scheme is an offline algorithm, which requires path planning and resource allocation through a specific ground station (such as QGroundControl in LINUX) before the mission is executed and does not need to run on UAVs.

4. Simulation Results

In this section, simulation results and some detailed discussions are provided. We first present the simulation settings and then analyze the effect of different energy budgets and the number of jammers on the experimental results. Finally, we compare the proposed algorithm with four baseline schemes to further illustrate the superiority of the joint trajectory planning, time, and power allocation scheme.

4.1. Simulation Settings

In the simulation, we considered a communication system with four UAV nodes, i.e., $k = 4$. In addition, it was assumed that the initial and end positions of the UAV 1–4 were $(200, 50)$, $(200, 70)$, $(200, 90)$, $(200, 110)$, and $(50, 50)$, $(50, 70)$, $(50, 90)$, $(50, 110)$, respectively. The rest of the parameter settings are shown in Table 1.

Table 1. Simulation Parameters Setting.

Parameter	Notation	Value
time slots	N	50
minimum safe distance	$D_{\min}$	10 m
Bandwidth	B	10 MHz
SN to UAV channel gain	β_{su}	−30 dB
Jammer to UAV channel gain	β_{Ju}	−60 dB
transmit power of SN	P_k	30 W
transmit power of jammer	P_j	5 W
energy collection efficiency	η	0.8
additive white Gaussian noise	σ^2	−169 dBm
UAV maximum speed	$V_{\max}$	10 m/s
the blade profile power	P_B	79.86 W
the induced power	P_I	88.63 W
the tip speed of the rotor blade	v_{tip}	120 m/s
the mean rotor induced velocity	v_0	4.03 m/s
the fuselage drag ratio	d_0	0.6
the air density	ρ	1.225 kg/m^3
the rotor solidity	s	0.05

4.2. Effect of Energy Budgets

Figure 4 shows the 2D trajectories of four UAVs with different energy budgets. We plotted the trajectories for $E_{th} = 10{,}000$ J, $E_{th} = 15{,}000$ J, and $E_{th} = 20{,}000$ J. It can be seen from Figure 4 that from four initial points, UAVs $1 - 4$ needed to approach the SNs according to the arc trajectory away from the jammers to ensure that more energy was collected to maximize the throughput of the DNs, and then fly back to the endpoints we set. For a different since the initial point was far from the source node, and in order to satisfy the minimum distance constraint between UAVs, it needed to fly a greater distance. Since UAV 4 was closest to the jammers, in order to ensure the communication quality, UAV 4 needed to be far away from the jammers under the constraint of the minimum safe distance and closer to the corresponding source node so as to collect more energy to communicate with the DN. Note that the UAVs cannot be infinitely close to the SNs, because while being closer to the SNs could guarantee enough energy to be collected, it would make the UAVs far away from the DNs, which would lead to the deterioration of the throughput. In addition, we noticed that the flying distance of the UAV increased with the energy budget, because a sufficient energy budget would ensure that the UAV was farther away from the jammers when planning a more reasonable path to maximize the throughput of the DN.

Figure 5 demonstrates the speed of four UAVs with different energy budgets. We observed that the UAVs' speed could be divided into two stages. In the first stage, the UAVs moved at high speed, and the speed decreased with time, but in the second stage, the UAVs accelerated to the endpoints. This is because in the first stage, the jammers were closer to the UAVs, and the UAVs needed to move away from the jammers at high speed to ensure communication quality. As the UAVs kept getting closer to the optimal positions, the speed needed to be reduced to collect more energy. However, due to the limited time, and energy budgets, the UAVs could not fly at low speed for a long time; thus, the UAVs needed to accelerate to the endpoints in the second stage. In addition, we can see that UAV 1 flew the fastest, while UAV 3 was the slowest. This is because UAV 1 was the farthest from its corresponding SN, and it needed to fly farther to collect more energy, while UAV 3 was the closest to its corresponding SN, so the budget was sufficient to allow it to collect the required energy with a lower speed. Finally, we observed that for the first 30 time slots and the last 10 time slots of the total mission, the UAVs' speed increased with energy budgets. That was because larger energy budgets could keep the UAVs away from the jammers and back to the endpoints at higher speed. These were as expected.
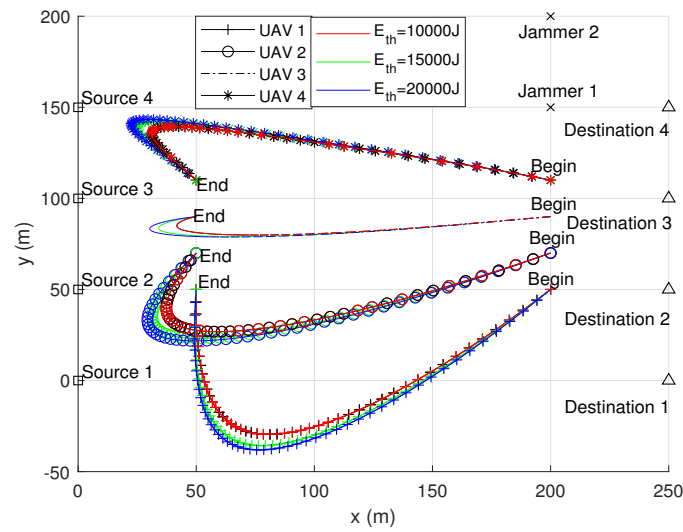
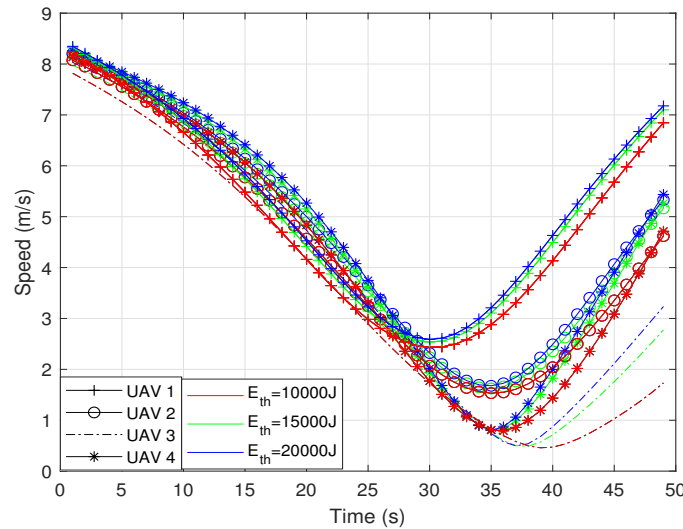**Figure 4.** Optimal trajectories in different energy budgets.

Figure 5. UAV's speed for different energy budgets.

Figure 6 and Figure 7 illustrate the variation of the power-splitting factor α and the time-allocation factor τ. It can be seen that α increased with time, and τ first increased and then decreased with time. This is because the UAVs moved away from the jammers and approached optimal points over time, at which point the SNs needed to consume less energy to ensure the SNR threshold constraint. As for τ, in the process of approaching the optimal points, τ first increased to ensure that enough energy was collected. When returning to the endpoints, in order to ensure the communication quality of the DNs, τ decreased to improve the throughput of the DNs.

Figure 8 presents the achievable throughput over every time slot. It is shown that the throughput increased first and then decreased. This was because the UAVs were initially far away from the jammers and closer to the optimal points, thereby collecting enough energy to increase the throughput. When returning to the endpoints, the throughput dropped as the UAVs moved away from the optimal points and closer to the jammers. Moreover, we noticed that the larger the UAV's energy budget, the greater the achievable throughput, which was in line with expectations.
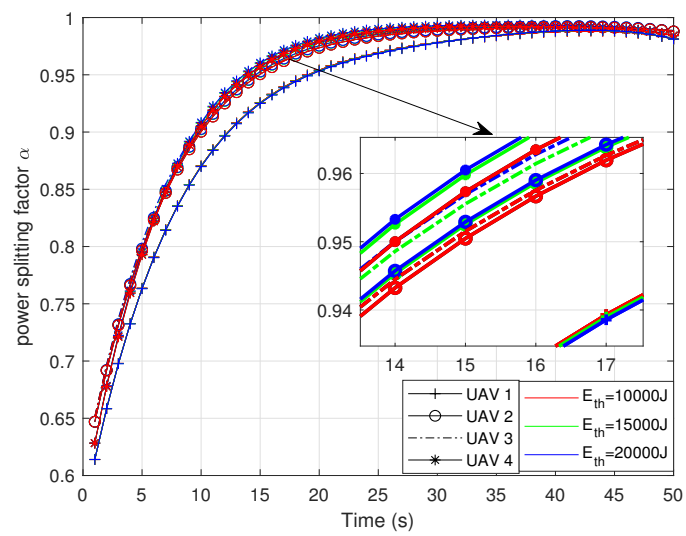
Figure 6. Power splitting factor in each time slot.
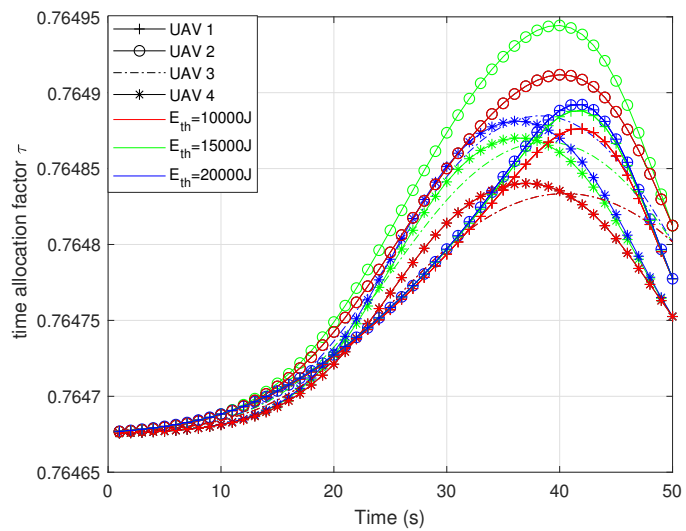
Figure 7. Time allocation factor in each time slot.
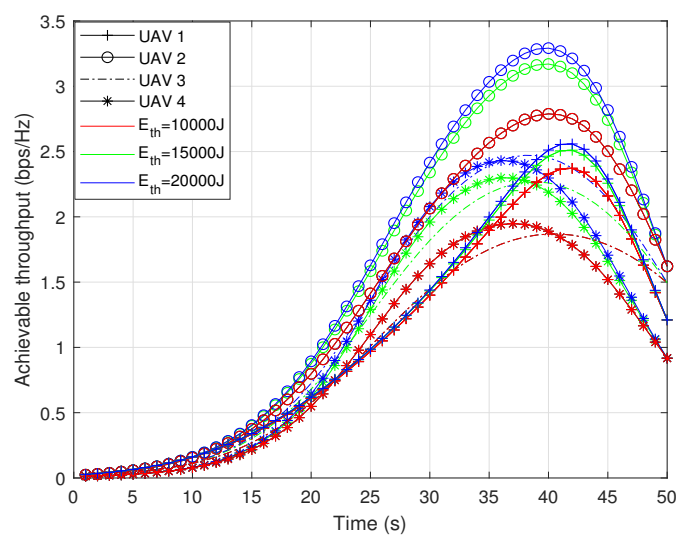
Figure 8. Achievable throughput over every time slot.

Furthermore, we increased the number of UAVs from 4 to 6, then 8 to further illustrate the performance of the proposed scheme. We set the initial and end positions of UAV 5–8 as (200, 240), (200, 260), (200, 280), and (200, 300); and (50, 240), (50, 260), (50, 280), and (50, 300), respectively. The achievable system throughput versus time is shown in Figure 9. It can be seen from Figure 9 that the throughput of the system increased with the number of UAVs. Given the energy budget, when $K = 8$, the throughput of the system was at the maximum; when $K = 2$, the throughput of the system was at the minimum. Moreover, it can be seen that given the number of UAVs, the throughput of the system increased with the energy budget. This was as expected.
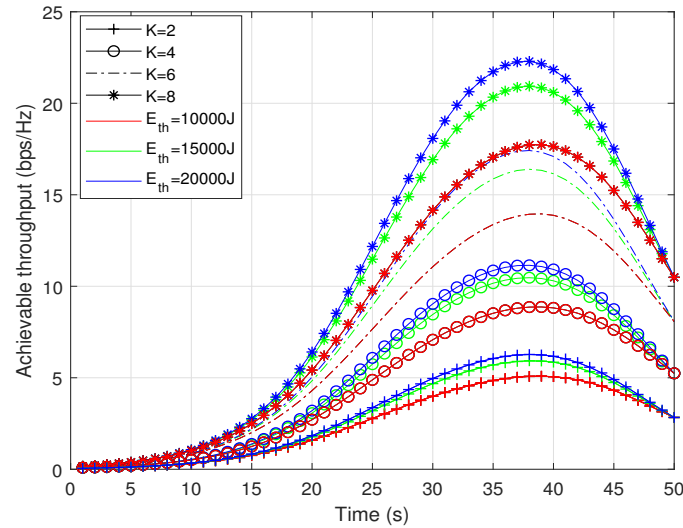
Figure 9. Achievable throughput over every time slot.

4.3. Effect of Jammers

Figure 10 shows the 2D trajectories of four UAVs with differing numbers of jammers. We plotted the trajectories for $J = 2$, $J = 3$, and $J = 4$. The basic trajectories of the four UAVs were consistent with those from Figure 4, and we will not repeat them here. It is worth noting that the flight distance of the UAVs increased with the number of jammers. Specifically, the more the number of jammers, the more obvious the interference effect, so the UAVs needed to be farther away from the jammers to ensure the channel throughput.
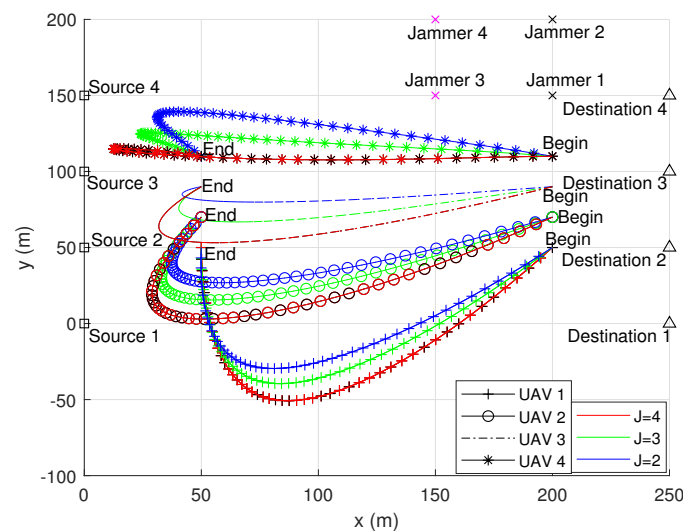

Figure 10. Optimal trajectories with different number of jammers.

Figure 11 displays the achievable throughput with different numbers of jammers. As can be seen from the figure, UAV 2 had the highest throughput. This is because UAV 2 was closer to the corresponding SN than UAV 1 and farther away from the jammers than UAV 3 and UAV 4. Finally, we observed that the throughput of all four UAVs decreased with the number of jammers. This was in line with our expectations and showed the significance of our study.
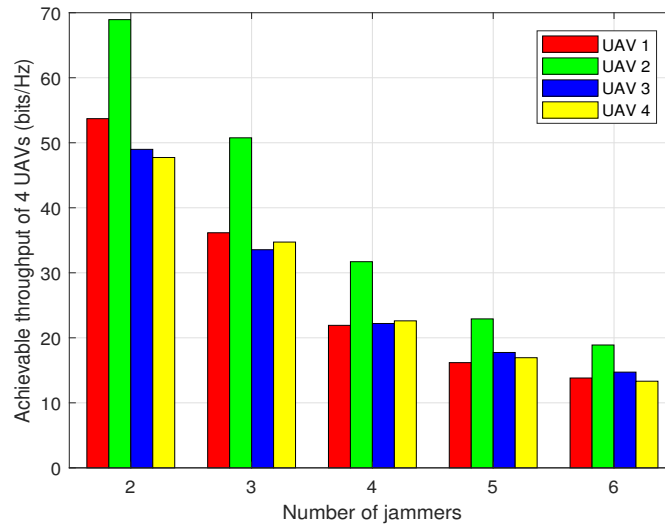

Figure 11. Achievable throughput with differing numbers of jammers.

Further, we increased the number of UAVs from 4 to 6, then 8 to further illustrate the impact of jammers on system performance. The achievable system throughput versus jammers is shown in Figure 12. As can be seen from Figure 12, the system throughput increased with the number of UAVs. Given the same number of jammers, when $K = 8$, the system throughput was at the maximum; when $K = 2$, the system throughput was at the minimum. Additionally, it can be seen that given the same number of UAVs, the throughput of the system decreased with the jammers. This was as expected.
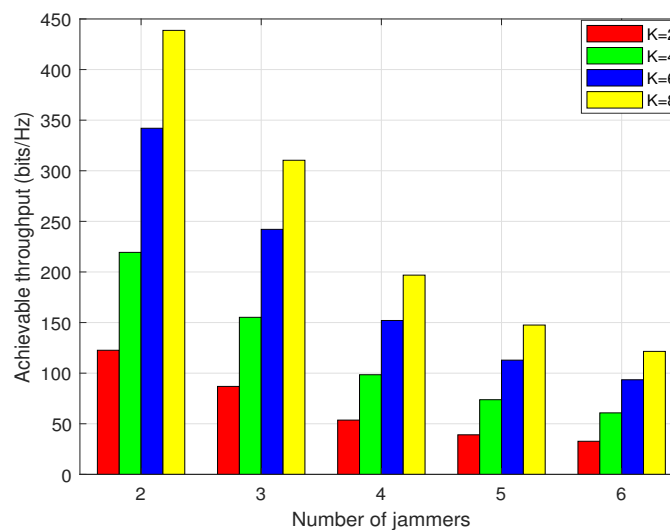

Figure 12. Achievable throughput with differing numbers of jammers.

4.4. Performance Comparison

In order to further illustrate the superiority of the proposed algorithm, in this subsection, we will compare our scheme with four baseline schemes:

- Scheme 1: Our proposed joint trajectory planning, time, and power allocation scheme.
- Scheme 2: Optimizing the power-splitting factor α and UAV's trajectory $\mathbf{Q}$ under the fixed time-allocation factor τ.
- Scheme 3: Optimizing the time-allocation factor τ and UAV's trajectory $\mathbf{Q}$ under the fixed power-splitting factor α.
- Scheme 4: Optimizing the UAV's trajectory $\mathbf{Q}$ under the fixed time-allocation factor τ and power-splitting factor α.
- Scheme 5: Optimizing the power-splitting factor α and time-allocation factor τ under circular trajectory.

We evaluated the average throughput of the two UAVs, as shown in Figure 13. For dynamic schemes 1–5, the throughput of the system first increased over time and then decreased as the UAVs moved away from the optimal positions and returned to the endpoints. Also, we noticed that scheme 5 had the worst performance since the circular trajectory had been set in advance. Moreover, at the best time slot, the average throughput of the proposed scheme 1 was two times higher than schemes 2 and 3.
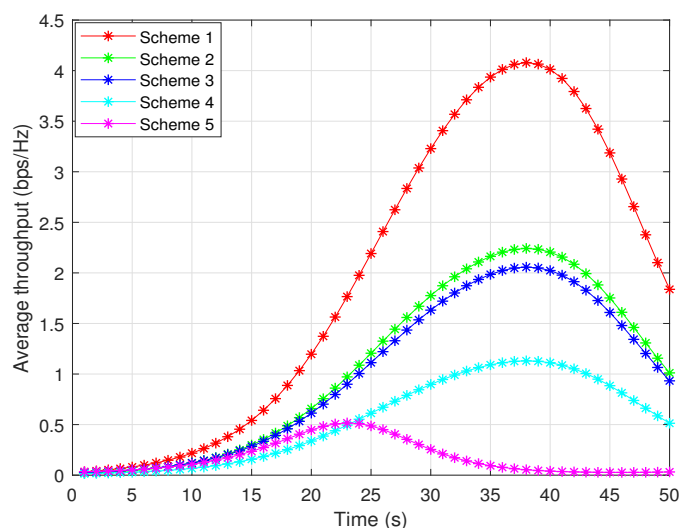

Figure 13. Average throughput in different schemes.

Figure 14 shows the average throughput with different energy budgets. It can be seen from Figure 14 that the average throughput of schemes 1–4 increased with the energy budget. For scheme 5, since the flight trajectory had been set in advance, increasing the energy budget did not bring about an improvement in average throughput. In addition, we observed that the proposed scheme 1 had the best performance, and the average throughput was increased by 40%, 50%, 150%, and 550% compared with schemes 2–5, respectively.

Figure 15 shows the average throughput of the system with differing number of jammers. Consistent with our expectations, the average throughput of all schemes decreased as the number of jammers increased. However, in comparison, the proposed scheme 1 had the best performance. Even in the extreme case with 6 jammers, the throughput of scheme 1 was still improved by 26%, 33%, 160%, and 500% compared with schemes 2–5.
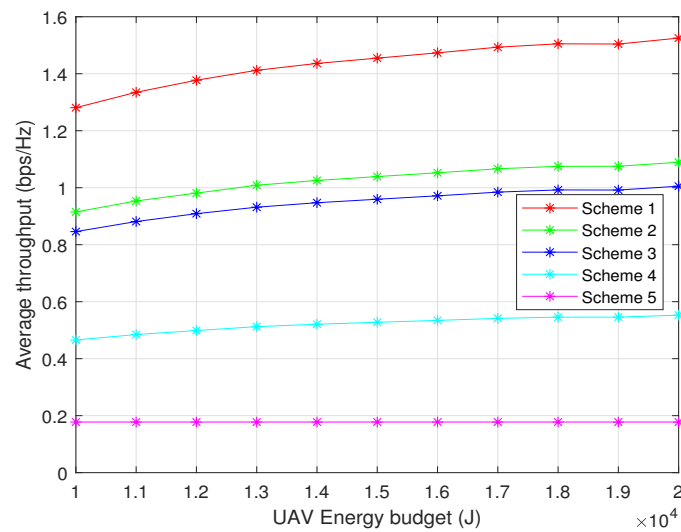
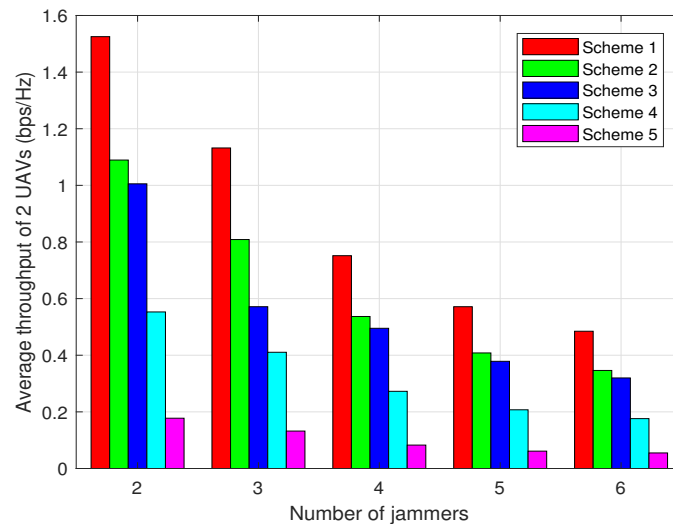**Figure 14.** Average throughput with different energy budgets.

Figure 15. Average throughput with differing numbers of jammers.

5. Conclusions

This paper investigated joint trajectory planning, time, and power resource allocation to maximize the throughput in UAV networks. Considering the limited energy budget of UAVs and the existence of multiple jammers, we introduced SWIPT technology to improve channel quality. Our goal was to maximize the throughput of the DNs. Since the original problem is non-convex, taking into account the actual flight constraints of the UAVs, we proposed an efficient joint optimization algorithm based on successive convex approximations, a block coordinate descent, and the slack variables method to obtain a suboptimal solution. Simulation results corroborated that the proposed scheme can significantly improve the channel throughput and illustrated the effectiveness of joint trajectory planning, time, and power allocation in mitigating interference. Finally, we compared the proposed scheme with four benchmark schemes to highlight the superiority of our study. In future work, we will consider the UAVs scenario with mobile nodes, more complex channel models, and/or scheduling schemes such as multi-UAV coordination and multi-point access.

Notations

The following notations are used in this manuscript:

Notation	Definition
$\mathbf{w}_{S_k}$	Location of the SN
$\mathbf{w}_{D_k}$	Location of the DN
$\mathbf{w}_j$	Locations of the jammer
Z	Height of the UAV
$\mathbf{q}_k$	Locations of the UAV
T	Total task time
N	Number of time slots
δ	Duration of each time slot
$V_{\max}$	The maximum speed of the UAV
$D_{\min}$	The minimum safe distance
$h_{S_k U_k}$	The channel-power gain between the SN and the UAV
$h_{j U_k}$	The channel-power gain between a jammer and a UAV
$h_{U_k D_k}$	The channel-power gain between a UAV and the DN
P_k	The transmit power of the SN
n_{su}	Additive white Gaussian noise
α	Power-splitting factor
τ	Time-allocation factor
η	Energy collection efficiency
P_B	The blade profile power
P_I	The induced power
v_{tip}	The tip speed of the rotor blade
v_0	The mean rotor induced velocity
d_0	The fuselage drag ratio
ρ	The air density
s	The rotor solidity
A_0	The rotor disc area

References

1. Xiang, C.; Li, Y.; Zhou, Y.; He, S.; Qu, Y.; Li, Z.; Gong, L.; Chen, C. A Comparative Approach to Resurrecting the Market of MOD Vehicular Crowdsensing. In Proceedings of the IEEE INFOCOM 2022—IEEE Conference on Computer Communications, London, UK, 2–5 May 2022; pp. 1479–1488.
2. Xiang, C.; Zhang, Z.; Qu, Y.; Lu, D.; Fan, X.; Yang, P.; Wu, F. Edge computing-empowered large-scale traffic data recovery leveraging low-rank theory. *IEEE Trans. Netw. Sci. Eng.* **2020**, *7*, 2205–2218. [CrossRef]
3. Ma, B.; Ren, Z.; Cheng, W. Traffic Routing-Based Computation Offloading in Cybertwin-Driven Internet of Vehicles for V2X Applications. *IEEE Trans. Veh. Technol.* **2021**, *71*, 4551–4560. [CrossRef]
4. Zhao, N.; Lu, W.; Sheng, M.; Chen, Y.; Tang, J.; Yu, F.R.; Wong, K.K. UAV-assisted emergency networks in disasters. *IEEE Wirel. Commun.* **2019**, *26*, 45–51. [CrossRef]
5. Jiang, X.; Sheng, M.; Zhao, N.; Xing, C.; Lu, W.; Wang, X. Green UAV communications for 6G: A survey. *Chin. J. Aeronaut.* **2022**, *35*, 19–34. [CrossRef]
6. Tran, D.H.; Vu, T.X.; Chatzinotas, S.; ShahbazPanahi, S.; Ottersten, B. Coarse trajectory design for energy minimization in UAV-enabled. *IEEE Trans. Veh. Technol.* **2020**, *69*, 9483–9496. [CrossRef]

7. Miao, J.; Wang, P. Power Control for Multi-UAV Location-aware Wireless Powered Communication Networks. In Proceedings of the 2020 IEEE/CIC International Conference on Communications in China (ICCC), Xiamen, China, 28–30 July 2020; pp. 225–230.

8. An K.; Liang, T.; Zheng, G.; Yan, X.; Li, Y.; Chatzinotas, S. Performance limits of cognitive-uplink FSS and terrestrial FS for Ka-band. *IEEE Trans. Aerosp. Electron. Syst.* **2018**, *55*, 2604–2611. [CrossRef]

9. An, K.; Lin, M.; Ouyang, J.; Zhu, W.-P. Secure Transmission in Cognitive Satellite Terrestrial Networks. *IEEE J. Sel. Areas Commun.* **2016**, *34*, 3025–3037. [CrossRef]

10. Zeng, Y.; Zhang, R. Energy-Efficient UAV Communication with Trajectory Optimization. *IEEE Trans. Wirel. Commun.* **2017**, *16*, 3747–3760. [CrossRef]

11. Lin, N.; Liu, Y.; Zhao, L.; Wu, D.O.; Wang, Y. An Adaptive UAV Deployment Scheme for Emergency Networking. *IEEE Trans. Wirel. Commun.* **2022**, *21*, 2383–2398. [CrossRef]

12. Ma, B.; Ren, Z.; Cheng, W. Credibility Computation Offloading Based Task-Driven Routing Strategy for Emergency UAVs Network. In Proceedings of the 2021 IEEE Global Communications Conference (GLOBECOM), Rio de Janeiro, Brazil, 4–8 December 2021; pp. 1–6.

13. Fu, Y.; Li, D.; Tang, Q.; Zhou, S. Joint Speed and Bandwidth Optimized Strategy of UAV-Assisted Data Collection in Post-Disaster Areas. In Proceedings of the 2022 20th Mediterranean Communication and Computer Networking Conference (MedComNet), Pafos, Cyprus, 1–3 June 2022; pp. 39–42.

14. Peer, M.; Bohara, V.A.; Srivastava, A. Multi-UAV Placement Strategy for Disaster-Resilient Communication Network. In Proceedings of the 2020 IEEE 92nd Vehicular Technology Conference (VTC2020-Fall), Virtual, 18 November–16 December 2020; pp. 1–7.

15. Kim, Y.H.; Chowdhury, I.A.; Song, I. Design and Analysis of UAV-Assisted Relaying with Simultaneous Wireless Information and Power Transfer. *IEEE Access* **2020**, *8*, 27874–27886. [CrossRef]

16. Zhan, C.; Hu, H.; Wang, Z.; Fan, R.; Niyato, D. Unmanned Aircraft System Aided Adaptive Video Streaming: A Joint Optimization Approach. *IEEE Transactions on Multimedia* **2020**, *22*, 795–807. [CrossRef]

17. Sun, Z.; Yang, D.; Xiao, L.; Cuthbert, L.; Wu, F.; Zhu, Y. Joint Energy and Trajectory Optimization for UAV-Enabled Relaying Network with Multi-Pair Users. *IEEE Trans. Cogn. Commun. Netw.* **2021**, *7*, 939–954. [CrossRef]

18. Gao, Y.; Wu, Y.; Cui, Z.; Yang, W.; Hu, G.; Xu, S. Robust trajectory and communication design for angle-constrained multi-UAV communications in the presence of jammers. *China Commun.* **2022**, *19*, 131–147. [CrossRef]

19. Feng, Z.; Ren, G.; Chen, J.; Zhang, X.; Luo, Y.; Wang, M.; Xu, Y. Power control in relay-assisted anti-jamming systems: A Bayesian three-layer Stackelberg game approach. *IEEE Access* **2019**, *7*, 14623–14636. [CrossRef]

20. Xu, Y.; Ren, G.; Chen, J.; Zhang, X.; Jia, L.; Feng, Z.; Xu, Y. Joint Power and Trajectory Optimization in UAV Anti-Jamming Communication Networks. In Proceedings of the ICC 2019—2019 IEEE International Conference on Communications (ICC), Shanghai, China, 20–24 May 2019; pp. 1–5.

21. Wu, Y.; Yang, W.; Guan, X.; Wu, Q. UAV-Enabled Relay Communication Under Malicious Jamming: Joint Trajectory and Transmit Power Optimization. *IEEE Trans. Veh. Technol.* **2021**, *70*, 8275–8279. [CrossRef]

22. Lin, Z.; An K.; Niu, H.; Hu, Y.; Chatzinotas, S.; Zheng, G.; Wang, J. SLNR-based Secure Energy Efficient Beamforming in Multibeam Satellite Systems. *IEEE Trans. Aerosp. Electron. Syst.* **2022**. [CrossRef]

23. Song, X.; Chang, Z.; Guo, X.; Wu, P.; Hämäläinen, T. Energy Efficient Optimization for Solar-Powered UAV Communications System. In Proceedings of the 2021 IEEE International Conference on Communications Workshops (ICC Workshops), Montreal, QC, Canada, 14–23 June 2021; pp. 1–6.

24. Sekander, S.; Tabassum, H.; Hossain, E. Statistical Performance Modeling of Solar and Wind-Powered UAV Communications. *IEEE Trans. Mob. Comput.* **2021**, *20*, 2686–2700. [CrossRef]

25. Mamaghani, M.T.; Hong, Y. Improving PHY-Security of UAV-Enabled Transmission with Wireless Energy Harvesting: Robust Trajectory Design and Communications Resource Allocation. *IEEE Trans. Veh. Technol.* **2020**, *69*, 8586–8600. [CrossRef]

26. Lu, W.; Fang, S.; Gong, Y.; Qian, L.; Liu, X.; Hua, J. Resource Allocation for OFDM Relaying Wireless Power Transfer Based Energy-Constrained UAV Communication Network. In Proceedings of the 2018 IEEE International Conference on Communications Workshops (ICC), Kansas City, MO, USA, 20–24 May 2018; pp. 1–6.

27. Ramzan, M.R.; Naeem, M.; Altaf, M.; Ejaz, W. Multi-Criterion Resource Management in Energy Harvested Cooperative UAV-enabled IoT Networks. *IEEE Internet Things J.* **2021**, *9*, 2944–2959. [CrossRef]

28. Wu, Y.; Yang, W.; Guan, X. UAV-UAV Communication Under Malicious Jamming: Trajectory Optimization with Turning Angle Constraint. In Proceedings of the 2020 International Conference on Wireless Communications and Signal Processing (WCSP), Nanjing, China, 21–23 October 2020; pp. 26–31.

29. Wang, X.; Gursoy, M.C.; Erpek, T.; Sagduyu, Y.E. Jamming-Resilient Path Planning for Multiple UAVs via Deep Reinforcement Learning. In Proceedings of the 2021 IEEE International Conference on Communications Workshops (ICC Workshops), Montreal, QC, Canada, 14–23 June 2021; pp. 1–6.

30. Zhou, L.; Zhao, X.; Guan, X.; Song, E.; Zeng, X.; Shi, Q. Robust trajectory planning for UAV communication systems in the presence of jammers. *Chin. J. Aeronaut.* **2022**, *35*, 265–274. [CrossRef]

31. Wu, Y.; Yang, W.; Guan, X.; Wu, Q. Energy-Efficient Trajectory Design for UAV-Enabled Communication Under Malicious Jamming. *IEEE Wirel. Commun. Lett.* **2021**, *10*, 206–210. [CrossRef]

32. Duo, B.; Luo, J.; Li, Y.; Hu, H.; Wang, Z. Joint trajectory and power optimization for securing UAV communications against active eavesdropping. *China Commun.* **2021**, *18*, 88–99. [CrossRef]
33. Li, X.; Xu, J. Positioning Optimization for Sum-Rate Maximization in UAV-Enabled Interference Channel. *IEEE Signal Process. Lett.* **2019**, *26*, 1466–1470. [CrossRef]
34. Wu, Y.; Fan, W.; Yang, W.; Sun, X.; Guan, X. Robust Trajectory and Communication Design for Multi-UAV Enabled Wireless Networks in the Presence of Jammers. *IEEE Access* **2020**, *8*, 2893–2905. [CrossRef]
35. Xiang, C.; Zhou, Y.; Dai, H.; Qu, Y.; He, S.; Chen, C.; Yang, P. Reusing delivery drones for urban crowdsensing. *IEEE Trans. Mob. Comput.* **2021**. [CrossRef]
36. Li, J.; Tian, Y.; Zhang, Y. Destination-Based Cooperative Jamming in Security UAV Relay System with SWIPT. In Proceedings of the 2021 13th International Conference on Communication Software and Networks (ICCSN), Chongqing, China, 4–7 June 2021; pp. 160–167.
37. Singh, R.; Rawat, M.; Jaiswal, A. On the Physical Layer Security of Mixed FSO-RF SWIPT System with Non-Ideal Power Amplifier. *IEEE Photonics J.* **2021**, *13*, 1–17. [CrossRef]
38. Wang, W.; Li, X.; Zhang, M.; Cumanan, K.; Ng, D.W.K.; Zhang, G.; Tang, J.; Dobre, O.A. Energy-constrained UAV-assisted secure communications with position optimization and cooperative jamming. *IEEE Trans. Commun.* **2020**, *68*, 4476–4489. [CrossRef]
39. Ji, B.; Li, Y.; Zhou, B.; Li, C.; Song, K.; Wen, H. Performance Analysis of UAV Relay Assisted IoT Communication Network Enhanced with Energy Harvesting. *IEEE Access* **2019**, *7*, 38738–38747. [CrossRef]
40. Park, J.C.; Kang, K.-M.; Choi, J. Low-Complexity Algorithm for Outage Optimal Resource Allocation in Energy Harvesting-Based UAV Identification Networks. *IEEE Commun. Lett.* **2021**, *25*, 3639–3643. [CrossRef]
41. Kumar, D.; Singya, P.K.; Bhatia, V. Performance Analysis of SWIPT Enabled Decode-and-Forward based Cooperative Network. In Proceedings of the 2022 IEEE 11th International Conference on Communication Systems and Network Technologies (CSNT), Indore, India, 23–24 April 2022; pp. 476–481.
42. Hu, T.; Ma, F.; Shang, Y.; Cheng, Y. Physical Layer Security of Untrusted UAV-enabled Relaying NOMA Network Using SWIPT and the Cooperative Jamming. In Proceedings of the 2021 IEEE 94th Vehicular Technology Conference (VTC2021-Fall), Virtual, 27 September–28 October 2021; pp. 1–6.
43. Najmeddin, S.; Bayat, A.; Aïssa, S.; Tahar, S. Energy-Efficient Resource Allocation for UAV-Enabled Wireless Powered Communications. In Proceedings of the 2019 IEEE Wireless Communications and Networking Conference (WCNC), Marrakesh, Morocco, 15–18 April 2019; pp. 1–6.
44. Su, Z.; Tang, J.; Feng, W.; Chen, Z.; Fu, Y.; Wong, K.-K. Energy Efficiency Optimization for D2D communications in UAV-assisted Networks with SWIPT. In Proceedings of the 2021 IEEE Global Communications Conference (GLOBECOM), Madrid, Spain, 7–11 December 2021; pp. 1–7.
45. Yang, Y.; Xiao, K. Energy Efficiency Optimization of Multi-user Distributed Antenna Systems with SWIPT Technique. In Proceedings of the 2021 International Conference on Communications, Information System and Computer Engineering (CISCE), Beijing, China, 14–16 May 2021; pp. 118–122.
46. Yang, H.; Ye, Y.; Chu, X.; Dong, M. Resource and Power Allocation in SWIPT-Enabled Device-to-Device Communications Based on a Nonlinear Energy Harvesting Model. *IEEE Internet Things J.* **2020**, *7*, 10813–10825. [CrossRef]
47. Zargari, S.; Hakimi, A.; Tellambura, C.; Herath, S. User Scheduling and Trajectory Optimization for Energy-Efficient IRS-UAV Networks with SWIPT. *IEEE Trans. Veh. Technol.* **2022**. [CrossRef]
48. Liu, Y.; Han, F.; Zhao, S. Flexible and Reliable Multiuser SWIPT IoT Network Enhanced by UAV-Mounted Intelligent Reflecting Surface. *IEEE Trans. Reliab.* **2022**, *71*, 1092–1103. [CrossRef]
49. Niu, H.; Chu, Z.; Zhu, Z.; Zhou, F. Aerial intelligent reflecting surface for secure wireless networks: Secrecy capacity and optimal trajectory strategy. *Intell. Converg. Netw.* **2020**, *3*, 119–133. [CrossRef]
50. Lin, Y.; Wang, T.; Wang, S. Trajectory Planning for Multi-UAV Assisted Wireless Networks in Post-Disaster Scenario. In Proceedings of the 2019 IEEE Global Communications Conference (GLOBECOM), Waikoloa, HI, USA, 9–13 December 2019; pp. 1–6.
51. Savkin, A.V.; Huang, C.; Ni, W. Joint Multi-UAV Path Planning and LoS Communication for Mobile Edge Computing in IoT Networks with RISs. *IEEE Internet Things J.* **2022**. [CrossRef]
52. Wang, L.; Wang, K.; Pan, C.; Xu, W.; Aslam, N.; Hanzo, L. Multi-Agent Deep Reinforcement Learning-Based Trajectory Planning for Multi-UAV Assisted Mobile Edge Computing. *IEEE Trans. Cogn. Commun. Netw.* **2021**, *7*, 73–84. [CrossRef]
53. Li, S.; He, C.; Liu, M.; Wan, Y.; Gu, Y.; Xie, J.; Fu, S.; Lu, K. Design and implementation of aerial communication using directional antennas: Learning control in unknown communication environments. *IET Control. Theory Appl.* **2019**, *13*, 2906–2916. [CrossRef]
54. Jayakody, D.N.K.; Perera, T.D.P.; Nathan, M.C.; Hasna, M. Self-energized Full-Duplex UAV-assisted Cooperative Communication Systems. In Proceedings of the 2019 IEEE International Black Sea Conference on Communications and Networking (BlackSeaCom), Sochi, Russia, 3–6 June 2019; pp. 1–6.
55. Boyd, S.; Boyd, S.P.; Vandenberghe, L. *Convex Optimization*; Cambridge University Press: Cambridge, UK, 2004.